



Scanning tunneling microscopy of MnO_x ultrathin films on Au(111)

Peiyu Chen^{a,b,*}, Yuhan Zhu^a, Tairu Ge^a, Martin R. Castell^{a,*}

^a Department of Materials, University of Oxford, Parks Road, Oxford OX1 3PH, United Kingdom

^b Department of Materials Science and Metallurgy, University of Cambridge, 27 Charles Babbage Road, Cambridge CB3 0FS, United Kingdom

ARTICLE INFO

Keywords:

Scanning tunneling microscopy
Manganese oxide
Ultrathin oxide films
Epitaxy
Hausmannite
Multiple image averaging

ABSTRACT

Two structurally distinct phases of manganese oxide ultrathin films were grown on Au(111) substrates and imaged at atomic resolution by scanning tunneling microscopy (STM). The so-called MnO_x *fishbone phase* is only a few monolayers thick and nucleates epitaxially on the bare Au(111) substrate. The surface of this phase exhibits two parallelogram unit cells with sizes and included angles of $(14.6 \pm 0.2) \times (5.6 \pm 0.2) \text{ \AA}^2$, $88 \pm 1^\circ$ and $(13.6 \pm 0.1) \times (5.6 \pm 0.2) \text{ \AA}^2$, $80 \pm 1^\circ$. The other thicker phase is called the *square phase*. It is only observed growing on top of the fishbone phase and has a surface unit cell of edge dimension $5.8 \pm 0.1 \text{ \AA}$. The square phase is thought to be a (001) termination of hausmannite Mn_3O_4 . In addition, less common intermediary surface structures are also observed. This study demonstrates the transition of the crystal structure of an oxide film from a unique ultrathin film structure that is epitaxially constrained by the interaction with the Au(111) substrate to that of a thicker film with the structure of a bulk crystal.

1. Introduction

Oxides of manganese (MnO_x) are one of the most widely studied transition metal oxides. They have been extensively explored for their catalytic properties in the oxygen evolution reaction [1], for CO activation [2], and in the removal of hazardous toluene from the atmosphere [3]. The chemical mechanisms underpinning the catalytic reactions depend on the surface atomic structure of MnO_x and the valence state of Mn [3–6]. It is therefore important to correlate the atomic and electronic structures of the oxide with its catalytic performance. A variety of stoichiometries and structures exist for MnO_x ($1 < x < 2$), among which Mn_3O_4 (hausmannite, with a spinel structure) is of particular research interest because of the mixed valence states of Mn (3+ and 2+) and the possibility of a variety of surface terminations. Mn_3O_4 growth has been studied on a range of crystalline substrates, each with a varying degree of influence on the terminations and atomic structures of Mn_3O_4 via the mechanisms of epitaxy and associated strain, e.g., $\text{SrTiO}_3(001)$ [7–9], $\text{SrTiO}_3(111)$ [9,10], $\text{Si}(001)$ [11,12], $\text{Ag}(001)$ [13–15], $\text{Pd}(001)$ [16], $\text{Cu}(111)$ [14,17,18], and $\text{Au}(111)$ [14,19–21]. The atomic and crystalline structures of the Mn_3O_4 films were investigated using X-ray diffraction (XRD) [7,8,10,12,21], reflection high energy electron diffraction (RHEED) [8], transmission electron microscopy (TEM) [12], atomic force microscopy (AFM) [7,10], scanning tunneling microscopy (STM) [15,17,19,20], scanning transmission electron

microscopy (STEM) [17], and low-energy electron diffraction (LEED) [13–15,17–19].

Among the studies listed above, only a few reported the surface atomic structures of Mn_3O_4 [15,17,19,20]. For example, Möller et al.'s STM study reported both a square structure and a few stripy patterns for $\text{Mn}_3\text{O}_4(001)$ grown on Au(111) [19]. The periodicity of the square pattern agreed with the lattice parameter of hausmannite $\text{Mn}_3\text{O}_4(001)$. The stripy patterns could not be resolved with certainty and were proposed to be surface reconstructions of $\text{Mn}_3\text{O}_4(001)$. Later in Liu et al.'s STM work, a stripy pattern was better resolved to show the Mn atoms, which was also proposed to be a Mn_3O_4 structure with a parallelogram unit cell [20]. Liu et al. also resolved the square pattern and thus determined the corresponding atomic structure with more confidence. In addition, there were some unidentified islands with a truncated triangular shape reported by Möller et al. formed upon vacuum annealing. Liu et al. later identified them as an $\text{MnO}(111)$ phase based on their atomically resolved STM images. These developments are a good example of how structural models can be refined and improved upon with higher resolution STM images.

Here, we report new STM data of MnO_x structures on Au(111) that demonstrates further atomic structure improvements of both the stripy and square patterns, which are surface terminations of two structurally different phases of MnO_x . The stripy pattern when imaged in STM with atomic resolution resembles “fishbones”, which adopts more than one

* Correspondence authors at: Department of Materials, University of Oxford, Parks Road, Oxford OX1 3PH, United Kingdom.

E-mail addresses: peiyu.chen@materials.ox.ac.uk (P. Chen), martin.castell@materials.ox.ac.uk (M.R. Castell).

<https://doi.org/10.1016/j.susc.2023.122248>

Received 1 November 2022; Received in revised form 23 December 2022; Accepted 9 January 2023

Available online 10 January 2023

0039-6028/© 2023 The Author(s). Published by Elsevier B.V. This is an open access article under the CC BY license (<http://creativecommons.org/licenses/by/4.0/>).

type of parallelogram unit cell. The “square” pattern, which exists only on thicker oxide layers, can be imaged to reveal individual atoms such that the structural solution can be further refined. The high quality of our STM images is achieved via both increased resolution of the raw images compared to previous studies and the use of multiple-image averaging to enhance the image signal-to-noise ratio (SNR).

2. Experimental techniques and procedures

Mica-supported Au(111) crystals were used as substrates (Unisoku Co., Ltd). They were sputtered by Ar⁺ ions (0.75–1 keV) for surface cleaning, followed by UHV annealing at 600 °C for 1.5 h resulting in the herringbone reconstruction. Mn (99.5% purity, Goodfellow, U.K.) was deposited onto the Au(111) substrates from an *e*-beam evaporator (Oxford Applied Research EGN4). When ~0.5 ML of Mn was oxidized in 1×10^{-6} Pa O₂ at 500 °C for 0.5–1 h, only the MnO_x fishbone phase was created. (The coverage of ~0.5 ML was estimated from the proportion of substrate covered by the fishbone islands.) When four times the amount (i.e., ~2 ML) of deposited Mn was oxidized under the same oxygen pressure and annealing conditions, the Mn₃O₄(001) square phase was also observed.

The samples were imaged by STM (JEOL JSTM 4500XT model, base pressure 10^{-8} Pa) at room temperature. STM images were processed by *Gwyddion*, *FabViewer* [22], and *Smart Align* [23,24]. *Smart Align* is a multi-frame averaging tool that helps to enhance the SNR in our STM images. It works by aligning multiple successive images of the same area and averaging them to calculate a “reference” image. Raw images are then corrected according to the reference image. The process can be repeated if necessary, using an updated “reference” image from the previous process. The availability of very high SNR data without the need for smoothing allows quantitative dimensional measurements to be taken with confidence. Most STM images shown in this work are averaged over 10–30 frames, while some small-scale ones are averaged over thousands of frames. This information is included in the figure captions.

3. Results and discussion

3.1. Fishbone phase

Fig. 1(a) shows a large-scale STM image of five islands with the

fishbone phase grown on Au(111). The stripes within the islands, which look like fishbones, align either with the Au(111) herringbones along the three $\langle 11\bar{2} \rangle$ directions, or with the three $\langle 1\bar{1}0 \rangle$ directions. Roughly 80% of the fishbones (stripes) align with $\langle 11\bar{2} \rangle$ directions [e.g., most islands in Fig. 1(a)], and around 20% align with the $\langle 1\bar{1}0 \rangle$ directions [e.g., the top left island in Fig. 1(a)]. The stripes show internal angles of 120° where the alignment changes direction. Note that the substrate lattice directions labeled in Fig. 1(a) do not apply to other panels as the images were taken on different parts of the Au (111) substrate, which is a polycrystal. In previous reports this fishbone structure has been interpreted as a Mn₃O₄ phase via the analysis of X-ray photoelectron spectroscopy (XPS) data [19,20].

Most of the fishbone islands observed in our experiments have an apparent thickness of ~2 Å as determined from STM measurements. Others are either ~3 Å or ~4 Å in thickness, as summarized in the histogram in Fig. 2. For example, most islands in Fig. 1(a) are ~2 Å thick, except for two of the islands towards the bottom of the figure which have an extra layer on part of them (the brighter parts), which are ~3 Å thick. Although the thinnest fishbone islands found in our study are ~2 Å, we believe they are not monolayers, as discussed later in relation to Fig. 1(c.ii).

Both Fig. 1(b.i) and 1(c.i) clearly show the fishbone pattern on the

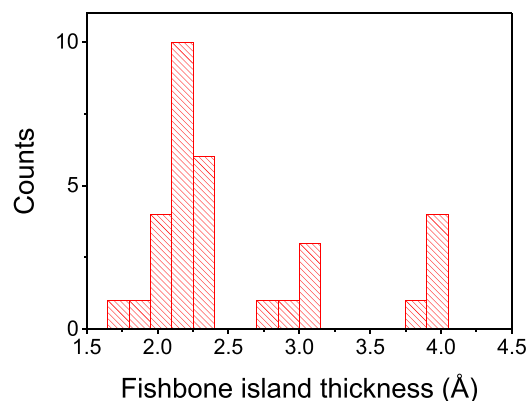


Fig. 2. Histogram of the thicknesses of fishbone MnO_x islands.

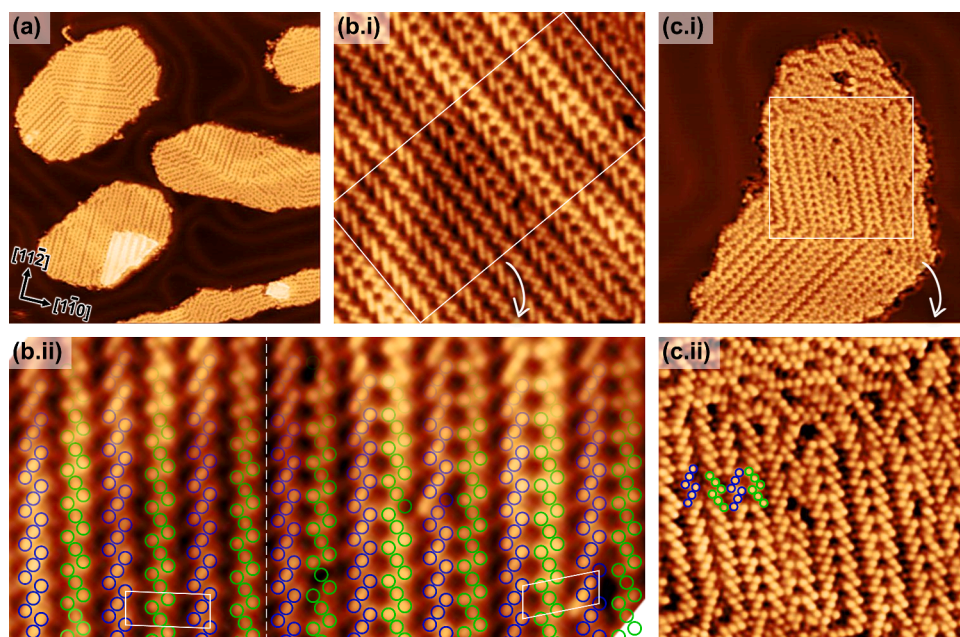


Fig. 1. STM images of the fishbone MnO_x islands grown on Au(111): (a) 43.1×43.1 nm², $V_s = 0.4$ V, $I_t = 0.80$ nA, averaged over 14 frames; (b.i) 11.2×11.2 nm², $V_s = 0.4$ V, $I_t = 0.80$ nA, averaged over 15 frames; (b.ii) close-up image of the boxed part in panel (b.i), averaged over 15 frames; (c.i) 21.0×21.0 nm², $V_s = 0.5$ V, $I_t = 0.50$ nA, averaged over 15 frames; (c.ii) close-up image of the boxed part in panel (c.i), averaged over 23 frames. In panels (b.ii) and (c.ii), each “fishbone” consists of a blue column and a green column, where the blue and green rings highlight the atomic positions. In (b.ii), two different parallelogram unit cells are identified for the patterns on the two sides of the vertical white dashed line.

MnO_x islands, and the areas in the white boxes are enlarged in Fig. 1(b.ii) and 1(c.ii), respectively. In Fig. 1(b.ii), atoms are circled in blue and green in alternating columns and each “fishbone” consists of a blue column and a green column. Within each column, atoms are grouped into threes. Here we cannot conclusively assign the atoms to be Mn or O, and we note that the structure shows no significant difference when imaged using positive and negative sample biases.

As can be seen from the large-scale image in Fig. 1(a), the spacing between neighboring fishbones is variable. Two types of periodicities are most commonly observed, which are both contained in Fig. 1(b.ii), separated by the vertical white dashed line. The atomic columns to the left of the dashed line are spaced further apart than those to the right, with a spacing of 14.6 ± 0.2 Å between adjacent blue columns on the left, and a spacing of 13.4 ± 0.1 Å on the right. Also, on the right, the blue and green columns within each fishbone are aligned with each other, while on the left, they are vertically offset. The unit cells in both cases are labeled by a white parallelogram. The left unit cell is $(14.6 \pm 0.2) \times (5.6 \pm 0.2)$ Å² in dimensions, with an included angle of $88 \pm 1^\circ$. The right unit cell is $(13.6 \pm 0.1) \times (5.6 \pm 0.2)$ Å² in dimensions, with an included angle of $80 \pm 1^\circ$. The periodicity in the vertical direction is the same in both patterns here and also in other less commonly observed patterns, i.e., the vertical spacing between neighboring sets of three-atom groups is always 5.6 ± 0.2 Å. While our right unit cell has not been previously reported, our left unit cell is consistent with the structure reported by Liu et al. [20], where they assigned a different unit cell for the same structure, which is a parallelogram with a more acute included angle (15.48×5.85 Å², 72°).

The island in Fig. 1(c.i) is measured to be ~ 2 Å thick, and we believe it is not a monolayer as Fig. 1(c.ii) shows atoms from the underlying layer as well. The two types of patterns analyzed in Fig. 1(b.ii) are also observed here, highlighted by a few groups of blue and green circles.

We believe that the complicated atomic arrangement of this fishbone phase and the six preferred epitaxial orientations are due to a strong interaction with the Au(111) substrate. One of the possible reasons for the multiple periodicities observed is that there are multiple sets of sites (i.e., combinations of hollow/bridge/atop sites) on the Au(111) substrate where Mn and O atoms can be favorably located. In addition to the epitaxial interaction, there is likely charge transfer from the MnO_x overlayers to the Au substrate because of the strong electronegativity of Au, which is another factor that can impact the structure and composition of the fishbone phase.

3.2. Square phase

When ~ 2 ML of Mn was oxidized under the same conditions as for the fishbone phase above (annealing in 1×10^{-6} Pa O₂ at 500 °C for 0.5–1 h), it resulted in a further dominant phase with a square unit cell, as shown by the black squares in Fig. 3. Another surface phase, which also has a square periodicity, but we think of as a transition phase, is shown in Fig. 3 with white squares.

The black squares represent a surface termination of a phase that has previously been identified as the hausmannite Mn₃O₄(001) phase in the literature [19,20]. The black squares in all panels in Fig. 3 have a measured edge length of 5.8 ± 0.1 Å, consistent with the lattice parameter of Mn₃O₄ ($a = b = 5.765$ Å). This phase was previously reported to form under more oxygen-lean conditions compared to the fishbone phase [20]. However, we found that the critical factor was the thickness of the layer rather than the oxygen annealing conditions. As can be seen in Fig. 3, the Au(111) substrate is completely covered by the fishbone phase, and the black square phase usually forms on top of the fishbone phase. Therefore, we believe that the fishbone phase is the nucleating phase and that the square phase only emerges after a certain thickness. The minimum thickness of the black square phase measured relative to the Au(111) substrate in our data is 5–6 Å (not shown in Fig. 3).

Each black square in Fig. 3 aligns one of its edges with the underlying

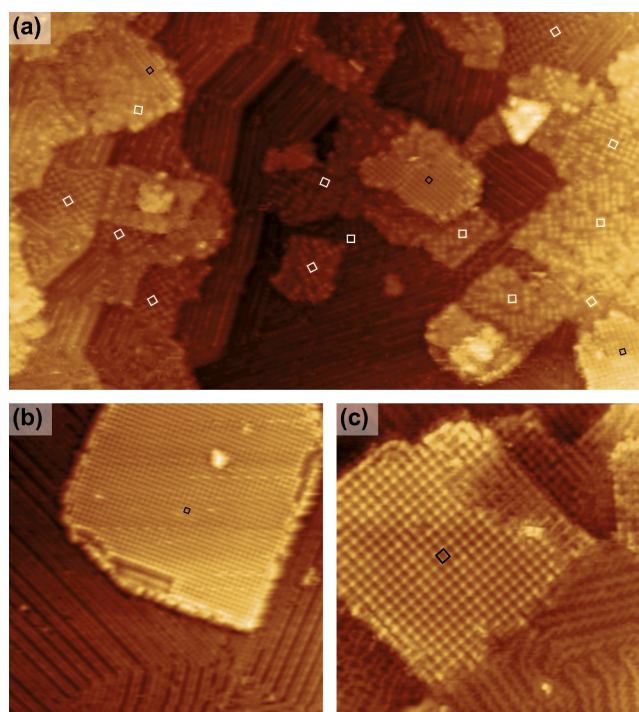


Fig. 3. STM images of two square phases: the black and white squares respectively have edge dimensions of 5.8 ± 0.1 Å and 8.1 ± 0.5 Å. Image sizes, scanning parameters, and *Smart Align* processing: (a) 70.0×41.2 nm², $V_s = 2.0$ V, $I_t = 0.25$ nA; (b) 37.1×37.1 nm², $V_s = 1.5$ V, $I_t = 0.20$ nA; (c) 18.0×18.0 nm², $V_s = 1.0$ V, $I_t = 0.20$ nA, averaged over 10 frames.

fishbone structure; this observation is the clearest in Fig. 3(b). Consistently, the black squares within a given sample area, e.g., in Fig. 3(a), all orient at 60° to each other. These orientations follow from the alignment of fishbones with the three $\langle 11\bar{2} \rangle$ directions and the three $\langle 1\bar{1}0 \rangle$ directions on Au(111), which are at 60° to each other.

The other square phase, represented by the white squares in Fig. 3(a), has a unit cell edge length of 8.1 ± 0.5 Å. This phase has also been reported previously, and was attributed to a $(\sqrt{2} \times \sqrt{2})R45^\circ$ reconstructed Mn₃O₄(001) surface [19,20]. Each of the black squares in Fig. 3 (a) can be associated with a white square rotated by 45° . The white squares themselves are oriented at 60° to each other. It can also be seen from Fig. 3(a) that the white square phase is generally less ordered with missing bright spots than the black square phase. In addition, the white square phase is sometimes observed to form on the same layer as the fishbone phase as seen for example in the top right corner of Fig. 3(a). We therefore believe that the white square phase is an intermediary structure that is part of a transition from the fishbone towards the black square phase. A further structure in the bottom left corner of Fig. 3(c) also seems to be a transition phase.

The Mn₃O₄(001) phase with a black square surface termination has steps of height 2.8 ± 0.3 Å, consistent with previously reported results [19]. This is significantly lower than the height of an orthorhombic unit cell of Mn₃O₄ ($c = 9.442$ Å). Since a full unit cell consists of eight atomic layers in the c direction [Fig. 4(c)], we believe our Mn₃O₄(001) layers are likely two atomic layers in thickness. This makes sense from a structural perspective because along the c axis of hausmannite Mn₃O₄, the more densely packed oxygen-containing layers are separated by a quarter of the c -axis unit cell dimension, i.e., 2.4 Å.

More details of the black square phase are shown in the STM images in Fig. 4. Slightly different patterns are resolved under positive [Fig. 4(a)] and negative [Fig. 4(b)] sample imaging biases. Note that Fig. 4(a) and (b) are not of the same area. STM images with an improved signal-to-noise ratio were obtained when thousands of unit cells were stacked and averaged using *Smart Align*, over 1561 and 2579 frames to produce

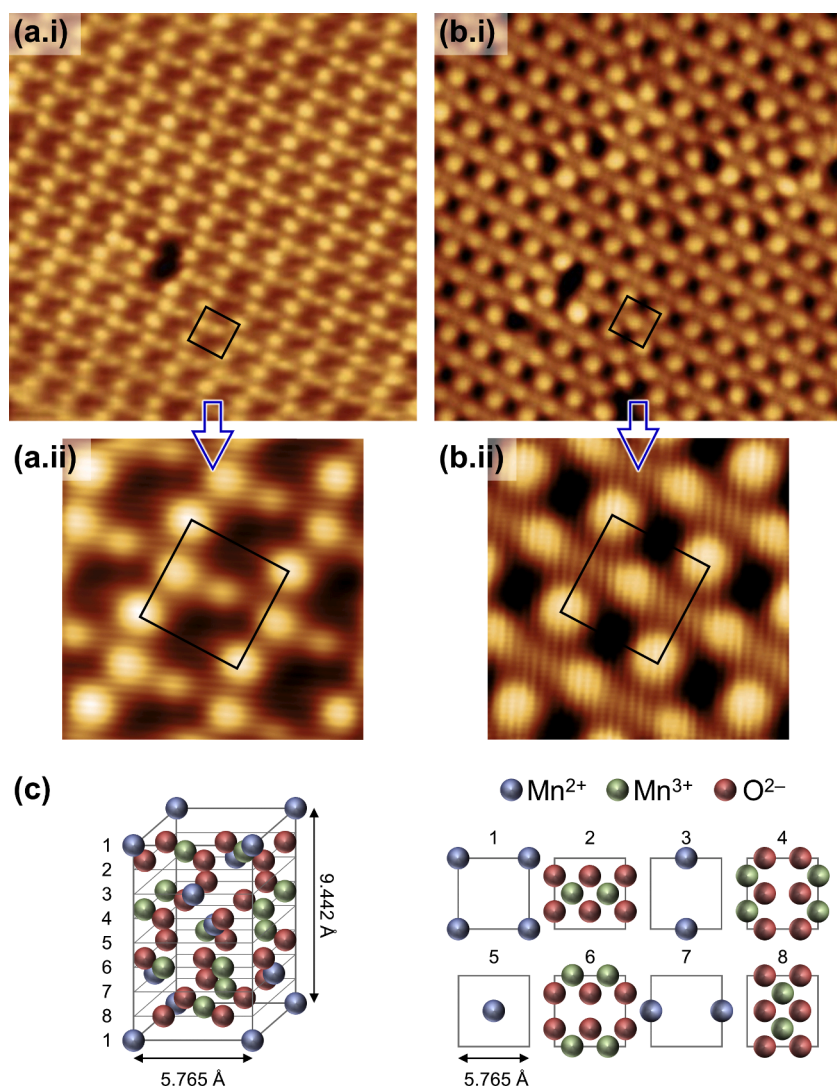


Fig. 4. STM images and atomic models of Mn₃O₄(001) islands (the black square phase) grown on Au(111). Panels (a) and (b) are empty-state and filled-state images, respectively. Panel (c) shows an orthorhombic unit cell of Mn₃O₄ and lays out the eight atomic layers perpendicular to the *c* direction. The square unit cell (edge length = 5.8 Å) is drawn in black or gray in all panels. Image sizes, scanning parameters, and *Smart Align* processing: (a.i) 6.3 × 6.3 nm², *V_s* = 1.0 V, *I_t* = 1.00 nA, averaged over 4 frames; (a.ii) close-up image of the unit cell in (a.i), averaged over 1561 frames; (b.i) 6.3 × 6.3 nm², *V_s* = -2.0 V, *I_t* = 0.50 nA, averaged over 12 frames; (b.ii) close-up image of the unit cell in (b.i), averaged over 2579 frames.

Fig. 4(a.ii) and 4(b.ii), respectively. In Fig. 4(a.ii), we can see four bright spots at the corners of the unit cell, as well as two less bright spots along the middle line of the unit cell. This unit cell could be a reconstruction formed by the superposition of layers 1 and 2 in Fig. 4(c) if the bright spots in the STM image correspond to Mn atoms, which, in the atomic model, are blue at the corners and green along the middle line of the unit cell. The structure in Fig. 4(b.ii) is similar to that in Fig. 4(a.ii), but the atoms along the middle line are shifted in position compared to the “green atoms” in the model, and the middle spot is much brighter. Further exploration of the atomic positions would require DFT simulations.

Our observations confirm the presence of an (001) termination of hausmannite Mn₃O₄, which is consistent with previous reports [19,20], though in previous reports, only the 5.8 Å periodicity was identified because of the limited STM resolution. The (001) layers of hausmannite Mn₃O₄ in the unit cell have alternating charges of +2 (Mn²⁺) and -2 (Mn³⁺O₄²⁻), meaning that a simple bulk termination is not possible. This means that the surface has to be reconstructed, although the reconstruction could be subtle. For example, it could involve atomic movements and changes in oxidation states that do not extend beyond a bulk (1 × 1) unit cell, therefore retaining the 5.8 Å periodicity. Future DFT models could be compared with our high-resolution STM data to determine the exact atomic configuration of the reconstruction.

The mechanisms that drive the fishbone-to-square phase transition are likely to initially involve a favored epitaxial interaction for the

nucleating fishbone phase. This phase is then retained for a few monolayers of growth, but beyond a critical thickness it transforms into the bulk form of hausmannite Mn₃O₄. The lowest energy termination of hausmannite is the (001) surface [25] and hence this determines this crystal surface orientation. It remains an open question as to whether the transition from the fishbone to the square hausmannite phase also causes the initial few monolayers of the fishbone phase to transform to hausmannite.

4. Conclusions

In summary, we have grown MnO_x ultrathin films on Au(111) substrates and have observed two phases with distinctly different surface structures. The MnO_x fishbone phase consists of a complicated atomic arrangement that results in a stripy pattern in STM images. This phase occurs for films of a few monolayers up to 4 Å in thickness and has preferred epitaxial orientations along the six <112̄> and <110̄> directions of the substrate. The fishbone phase is stabilized by the interaction with the Au(111) substrate and does not appear to have a bulk analog. For thicker films that are at least 5–6 Å thick, we observe a square phase which appears to have the structure of hausmannite Mn₃O₄ with a reconstructed (001) termination. For both the fishbone and square phases, our STM images show multiple features within the surface unit cells with a high signal-to-noise ratio due to multiple image averaging. These images provide the necessary high-resolution

information that is required for comparison with future DFT simulations of the reconstructions. This will enable the atomic surface structures to be determined and form an underpinning link to the understanding of the catalytic activity of these manganese oxides.

CRedit authorship contribution statement

Peiyu Chen: Formal analysis, Investigation, Data curation, Writing – original draft, Writing – review & editing, Visualization. **Yuhan Zhu:** Conceptualization, Methodology, Validation, Formal analysis, Investigation, Data curation. **Tairu Ge:** Methodology, Validation, Formal analysis, Investigation, Data curation. **Martin R. Castell:** Conceptualization, Methodology, Validation, Resources, Writing – review & editing, Supervision, Project administration, Funding acquisition.

Declaration of Competing Interest

The authors declare that they have no known competing financial interests or personal relationships that could have appeared to influence the work reported in this paper.

Data Availability

Data will be made available on request.

Acknowledgments

The authors would like to thank Chris Spencer (JEOL U.K.) for technical support. YZ is grateful to the China Scholarship Council (CSC) for financial support.

References

- [1] D.M. Robinson, Y.B. Go, M. Mui, G. Gardner, Z. Zhang, D. Mastrogiovanni, E. Garfunkel, J. Li, M. Greenblatt, G.C. Dismukes, Photochemical water oxidation by crystalline polymorphs of manganese oxides: structural requirements for catalysis, *J. Am. Chem. Soc.* 135 (2013) 3494–3501, <https://doi.org/10.1021/ja310286h>.
- [2] Y. Li, L. Lin, R. Mu, Y. Liu, R. Zhang, C. Wang, Y. Ning, Q. Fu, X. Bao, Activation of CO over ultrathin manganese oxide layers grown on Au(111), *ACS Catal.* 11 (2021) 849–857, <https://doi.org/10.1021/acscatal.0c04302>.
- [3] Y. Lyu, C. Li, X. Du, Y. Zhu, Y. Zhang, S. Li, Catalytic removal of toluene over manganese oxide-based catalysts: a review, *Environ. Sci. Pollut. Res.* 27 (2020) 2482–2501, <https://doi.org/10.1007/s11356-019-07037-2>.
- [4] S. Zhu, J. Wang, L. Nie, Progress of catalytic oxidation of formaldehyde over manganese oxides, *ChemistrySelect* 4 (2019) 12085–12098, <https://doi.org/10.1002/slct.201902701>.
- [5] Z. Ye, J.M. Giraudon, N. De Geyter, R. Morent, J.F. Lamonier, The design of MnOx based catalyst in post-plasma catalysis configuration for toluene abatement, *Catalysts* 8 (2018) 91, <https://doi.org/10.3390/catal8020091>.
- [6] S. Rong, P. Zhang, F. Liu, Y. Yang, Engineering crystal facet of α -MnO₂ nanowire for highly efficient catalytic oxidation of carcinogenic airborne formaldehyde, *ACS Catal.* 8 (2018) 3435–3446, <https://doi.org/10.1021/acscatal.8b00456>. Research.
- [7] S. Huang, Y. Wang, Z. Wang, K. Zhao, X. Shi, X. Lai, L. Zhang, Structural, magnetic and magnetodielectric properties of the Mn₃O₄ thin films epitaxially grown on SrTiO₃ (001) substrates, *Solid State Commun.* 212 (2015) 25–29, <https://doi.org/10.1016/j.ssc.2015.04.004>.
- [8] G. Wang, S. Wu, W. Zhou, Y. Wang, S. Li, Novel magnetic properties of single-crystalline Mn₃O₄ (004) film grown on SrTiO₃ (001) substrate by molecular beam epitaxy, *Mater. Lett.* 195 (2017) 86–88, <https://doi.org/10.1016/j.matlet.2017.02.085>.
- [9] K.A. Bogle, V. Anbusathaiah, M. Arredondo, J.-Y. Lin, Y.-H. Chu, C. O'Neill, J. M. Gregg, M.R. Castell, V. Nagarajan, Synthesis of epitaxial metal oxide nanocrystals via a phase separation approach, *ACS Nano* 4 (2010) 5139–5146, <https://doi.org/10.1021/nn1010123>.
- [10] L. Bigiani, C. Maccato, A. Gasparotto, C. Sada, D. Barreca, Structure and properties of Mn₃O₄ thin films grown on single crystal substrates by chemical vapor deposition, *Mater. Chem. Phys.* 223 (2019) 591–596, <https://doi.org/10.1016/j.matchemphys.2018.11.047>.
- [11] L. Bigiani, D. Barreca, A. Gasparotto, C. Maccato, Mn₃O₄ thin films functionalized with Ag, Au, and TiO₂ analyzed using x-ray photoelectron spectroscopy, *Surf. Sci. Spectra.* 25 (2018) 14003, <https://doi.org/10.1116/1.5029889>.
- [12] L. Bigiani, M. Hassan, D. Peddis, C. Maccato, G. Varvaro, C. Sada, E. Bontempi, S. Martí-Sa, J. Arbiol, D. Barreca, High magnetic coercivity in nanostructured Mn₃O₄ thin films obtained by chemical vapor deposition, *ACS Appl. Nano Mater.* 2 (2019) 1704–1712, <https://doi.org/10.1021/acsnm.9b00141>.
- [13] A.K. Kundu, S. Barman, K.S.R. Menon, Stabilization of polar Mn₃O₄(001) film on Ag(001): interplay between kinetic and structural stability, *Surf. Sci.* 664 (2017) 207–215, <https://doi.org/10.1016/j.susc.2017.06.017>.
- [14] E. Annese, A. Ali, J. Barreto, G. Felix, F. Stavale, Unraveling hausmannite (Mn₃O₄) thin films surface structure by X ray linear dichroism, *Appl. Surf. Sci.* 578 (2022), 151944, <https://doi.org/10.1016/j.apsusc.2021.151944>. Contents.
- [15] K. Gillmeister, M. Trautmann, M. Huth, R. Shantyr, K. Meinel, A. Chassé, K.-M. Schindler, H. Neddermeyer, W. Widdra, Surface reconstructions on Mn₃O₄ (001) film, *Phys. Rev. B* 105 (2022), 195415, <https://doi.org/10.1103/PhysRevB.105.195415>.
- [16] C. Franchini, J. Zabloudil, R. Podloucky, F. Allegretti, F. Li, S. Surnev, F.P. Netzer, Interplay between magnetic, electronic, and vibrational effects in monolayer Mn₃O₄ grown on Pd(100), *J. Chem. Phys.* 130 (2009), 124707, <https://doi.org/10.1063/1.3097957>.
- [17] R. Caetano, A. Ali, J. Barreto, G. Félix, M.I. Ramos, B.S. Archanjo, C.A. Achete, E. Annese, F. Stavale, The structure of Mn₃O₄ (110) thin films, *Surf. Sci.* 720 (2022), <https://doi.org/10.1016/j.susc.2022.122062>, 122062 Contents.
- [18] E. Annese, A. Ali, J. Barreto, F. Stavale, Mn₃O₄ thin film on Cu(111): modulating electronic structure through film–substrate interaction, *J. Phys. Chem. C* 124 (2020) 15162–15170, <https://doi.org/10.1021/acs.jpcc.0c01961>.
- [19] C. Möller, J. Barreto, F. Stavale, N. Nilius, Manganese oxide thin films on Au(111): growth competition between MnO and Mn₃O₄, *J. Phys. Chem. C* 123 (2019) 7665–7672, <https://doi.org/10.1021/acs.jpcc.8b04176>.
- [20] Y. Liu, R. Zhang, Y. Ling, L. Lin, R. Mu, Q. Fu, Dynamic structural evolution of Mn–Au alloy and MnOx nanostructures on Au(111) under different atmospheres, *J. Phys. Chem. C* 125 (2021) 15335–15342, <https://doi.org/10.1021/acs.jpcc.1c04195>.
- [21] Y. Li, L. Lin, L. Gao, R. Mu, Q. Fu, X. Bao, Predominance of subsurface and bulk oxygen vacancies in reduced manganese oxide, *J. Phys. Chem. C* 125 (2021) 7990–7998, <https://doi.org/10.1021/acs.jpcc.1c01203>.
- [22] F. Silly, A robust method for processing scanning probe microscopy images and determining nanoobject position and dimensions, *J. Microsc.* 236 (2009) 211–218, <https://doi.org/10.1111/j.1365-2818.2009.03191.x>.
- [23] L. Jones, S. Wang, X. Hu, S. ur Rahman, M.R. Castell, Maximising the resolving power of the scanning tunneling microscope, *Adv. Struct. Chem. Imaging* 4 (2018) 7, <https://doi.org/10.1186/s40679-018-0056-7>.
- [24] L. Jones, H. Yang, T.J. Pennycook, M.S.J. Marshall, S. Van Aert, N.D. Browning, M. R. Castell, P.D. Nellist, Smart align—a new tool for robust non-rigid registration of scanning microscope data, *Adv. Struct. Chem. Imaging* 1 (2015) 8, <https://doi.org/10.1186/s40679-015-0008-4>.
- [25] P.R. Garcês Gonçalves, H.A. De Abreu, H.A. Duarte, Stability, structural, and electronic properties of hausmannite (Mn₃O₄) surfaces and their interaction with water, *J. Phys. Chem. C* 122 (2018) 20841–20849, <https://doi.org/10.1021/acs.jpcc.8b06201>.